Journal of
Nanoscience and Nanotechnology
Vol. 8, 1979-1988, 2008

Nano-Sized Ceramic Inks for Drop-on-Demand Ink-Jet Printing in Quadrichromy

Davide Gardini[1], Michele Dondi[1,*], Anna Luisa Costa[1], Francesco Matteucci[1], Magda Blosi[1], Carmen Galassi[1], Giovanni Baldi[2], and Elenia Cinotti[2]

[1]*CNR-ISTEC, Institute of Science and Technology for Ceramics, Via Granarolo 64, 48018 Faenza, Italy*
[2]*CERICOL, Centro Ricerche Colorobbia, Via Pietramarina 53, 50053 Sovigliana Vinci, Italy*

Nano-sized ceramic inks suitable for ink-jet printing have been developed for the four-colours CMYK (cyan, magenta, yellow, black) process. Nano-inks of different pigment composition ($Co_{1-x}O$, Au^0, TiO_2:Sb,Cr, $CoFe_2O_4$) have been prepared with various solid loadings and their chemico-physical properties (particle size, viscosity, surface tension, ζ-potential) were tailored for the ink-jet application. The pigment particle size is in the 20–80 nm range. All these nano-suspensions are stable for long time (i.e., several months) due to either electrostatic (high ζ-potential values) or steric stabilization mechanisms. Both nanometric size and high stability avoid problems of nozzle clogging from particles agglomeration and settling. Nano-inks have a Newtonian behaviour with relatively low viscosities at room temperature. More concentrated inks fulfil the viscosity requirement of ink-jet applications (i.e., $<$35 mPa $\cdot$ s) for printing temperatures in between 30 and 70 °C. Surface tension constraints for ink-jet printing are fulfilled by nano-inks, being in the 35–45 mN $\cdot$ m^{-1} range. The nano-sized inks investigated behave satisfactorily in preliminary printing tests on several unfired industrial ceramic tiles, developing saturated colours in a wide range of firing temperatures (1000–1200 °C).

Keywords: Ceramic Ink, Ink-Jet Printing, Nanopigment, Rheological Properties

RESEARCH ARTICLE

1. INTRODUCTION

Decoration is aimed at increasing the aesthetic value of surfaces and in the manufacturing of consumer products its improvement is pivotal.[1] Ink-jet printing is a non-impact method based on projecting ink droplets onto a surface.[2–3] Two main types of ink-jet printers are widely used: *continuous* and impulse or *drop on demand* (DOD). In continuous printers the ink stream, once ejected from the orifice, is broken in droplets that are first selectively electrically charged, then—passing through an electrical field—the charged droplets are deflected in a gutter for recirculation, while the uncharged ones directly spread on the substrate to form an image.[2–3] As far as DOD printers are concerned, ink droplets are ejected, only when required, by the application of an electrical signal to the piezoelectric actuator that, by a mechanical displacement, squeezes out the droplets.[3–4]

Many characteristics of ink-jet printing technology make it interesting for decoration of ceramic articles. In particular, as far as high resolution images are concerned, owing to the very small volume involved in the ink-jet technology in comparison to other decorating technologies, a better control of image quality is achieved. Besides, customized products can be obtained at acceptable costs, especially when the quadrichromy process is used, implying four basic colours: cyan, magenta, yellow and black (CMYK). In fact, the change of the image is obtained without any substitution of mechanical parts, like in the other decoration technologies, but only through the change of the software input.

Nevertheless, ink-jet printing has been applied to ceramic decoration since a few years and up to now it has not become a common technology in the ceramic industry.[5–6] This delay is due to the severe requirements concerning both ceramic pigments and inks. In particular, colorants for ceramic materials must be highly refractory, capable to withstand the chemical corrosion of liquid phases formed during the firing of bodies or glazes, and with suitable optical characteristics.[7–9] On the other hand, the quality of the ink-jet image depends on the properties of inks (i.e., viscosity, surface tension) and substrates (e.g., composition, porosity) and on their interaction (i.e., wettability, spreading, penetration).[10–13] In any case, the control and optimisation of the ink physical properties, such as

*Author to whom correspondence should be addressed.

viscosity and surface tension, are the most critical issues for the ink-jet printing technology.[4, 10, 13] Ink viscosity must be low enough to allow a fast flow through the nozzles of printhead, under the pressure gradient arising from the displacement of the piezoelectric actuator, and to enhance the penetration in the capillary channels of porous substrate. Surface tension must be in the 35–45 $mN \cdot m^{-1}$ range, in order to avoid ink spreading over the nozzle as well as any spilling out of the orifice by gravity.[3, 10]

Nowadays, ink-jet printing on ceramic tiles is carried out by using either organometallic dyes (the so-called *soluble salts*) or conventional ceramic pigments ground down to submicrometric sizes.[8] Soluble salts suffer for a limited colour palette and insufficient chromatic saturation; their use brings about environmental constraints.[8] Micronized pigments can cause nozzles clogging and are affected by dispersion instability (i.e., settling) and a loss of colour strength.[14] These problems can be overcome by using nano-sized ceramic inks (*nano-inks*) i.e., dispersions of nanometric particles in a liquid organic vehicle, that are able to increase the image quality ensuring high reliability to the printing systems.[15] As well known from the literature, nanoscale crystalline materials can be synthesized through the so-called polyol process.[16–20] The nano-inks concerned in the present investigation were obtained through a modified polyol procedure patented by Colorobbia Italia.[21]

This work is aimed at developing nano-inks suitable for DOD ink-jet printing. The rationale was synthesizing ceramic inks able to impart the four basic colours (cyan, magenta, yellow and black: CMYK) tailoring their chemical and physical properties to fulfil the DOD requirements by adding proper additives and/or changing operating conditions.

RESEARCH ARTICLE

2. EXPERIMENTAL DETAILS

2.1. Materials

Nano-inks were prepared by CERICOL in the form of suspensions of ceramic oxides or metals synthesized in an organic medium. The syntheses were pursued by a specifically modified polyol procedure in which the metal precursors are dispersed in glycol and the batch heated over 150 °C.[21] The composition, pigment density and solid content of inks are summarized in Table I. In order to study the effect of pigment concentration, the Yellow and Black inks were prepared with different solid loadings ranging nominally from 1 to 12 wt%.

All the nano-inks are very stable over time, as no phase separation and colour change occurred in the samples stored for several months.

2.2. Particle Size Distribution

The particle size distribution of pigment dispersed in the glycol was appraised by different techniques. As prepared inks, poured into a quartz cuvette, were measured by Dynamic Light Scattering (DLS, ZetaSizer-NanoSeries, Malvern Instruments, Malvern, UK), while dried powders placed on a metallic grid were analysed by Transmission Electron Microscopy (TEM, Zeiss 109, Oberkochen, Germany) performed at 80 kV and by Scanning Electron Microscopy equipped with a field emission gun (SEM-FEG and STEM, Supra40, Zeiss, Oberkochen, Germany) performed at 20 kV. As the light absorbance of the DLS instrument is in the blue region, the Cyan ink was analysed by SEM-FEG only.

2.3. Phase Composition

The pigment phase composition was determined through high temperature X-ray powder diffraction (HT-XRPD) carried out with a Pananalytical X'Pert Pro goniometer (Almelo, The Netherlands) using graphite-monochromated Cu $K_{1,2}$ radiation, 10–80° 2θ range, scan rate 0.02°, 3 s per step, heating the sample up to 700 °C; the quantitative interpretation of XRD patterns was performed by the Rietveld method with the GSAS-EXPGUI software package.[22–23]

2.4. Shear Viscosity

The shear viscosity of nano-inks was measured by a stress-controlled rotational rheometer equipped with a plate–plate geometry (Bohlin C-VOR 120, Malvern-Bohlin Instruments, Cirencester, UK). The diameter of the plates was 60 mm and the gap imposed between the plates was 500 μm. Flow curves at 25 °C were determined increasing the shear stress from 0.1 to 10 Pa in 21 logarithmic steps and measuring the corresponding shear rates. The effect of temperature on the shear viscosity was investigated increasing the temperature from 25 to 85 °C at a rate of 1 $°C \cdot min^{-1}$ (keeping the inks in flow at 10 s^{-1} of shear rate).

2.5. Surface Tension

The surface tension of nano-inks was determined with an optical device provided with a CCD video camera with a resolution of 752 × 582 pixels and a rate of image acquisition of 25 frames per second (OCA 15+, DataPhysics Instruments, Filderstadt, Germany). The pendant drop method was used with flat needles of 1.65 mm of outer diameter. An image acquisition software allowed to determine the outline of the hanging nano-ink drops, which were fitted by the Laplace-Young method. The calculation of the surface tension requires the knowledge of the material density, which was previously measured by the gravimetric method. The fitting was performed on well-developed droplets (of about 14 μL of volume) hung to the needle. In order to determine the dependence of surface tension of nano-inks on temperature, it was measured in a thermal chamber (TFC 100) at four temperatures (25, 40, 60 and 70 °C) controlled by circulating thermostated water.

Table I. Physical and chemical properties of nano-inks.

Property	Unit	Nano-ink			
		Cyan	Magenta	Yellow	Black
Pigment stoichiometry		$Co_{1-x}O$	Au^0	TiO_2:Sb, Cr	$CoFe_2O_4$
Pigment density	$g \cdot cm^{-3}$	6.25	19.32	4.25	5.27
Ink density	$g \cdot cm^{-3}$	1.14	1.12	1.26	1.23
Solid loading	wt%	4.0	1.0	12.0	12.9
Solid loading	vol.%	0.74	0.06	3.47	3.05
Particle size (DLS)	nm	n.d.	74	19	22
Particle size (TEM, STEM, SEM-FEG)	nm	$10 \div 20$	$20 \div 40$	$10 \div 20$	$20 \div 30$
Viscosity (25 °C)	mPa · s	38.8	42.0	185	56.7
Surface tension (25 °C)	$mN \cdot m^{-1}$	44.0	37.3	40.8	38.8
ζ-potential	mV	4.4[a]	91.1[b]	20.3[c]	47.5[a]
Electric conductivity	$\mu S \cdot cm^{-1}$	10	1420	88	15

ζ-potential: [a]Attenuation, [b]ESA, [c]Hückel. n.d. = not determined.

2.6. ζ-Potential and Electric Conductivity

The ζ-potential of pigments was measured by an electroacoustic technique (AcoustoSizer II, Colloidal Dynamics, Warwick, USA) based on the measure of the Electrokinetic Sonic Amplitude (ESA) signal generated in the colloidal systems.[22–25] The ESA signal is an electrokinetic effect, generated by the motion of charged particles dispersed in a liquid when an alternate electric field is applied, that is related to the ζ-potential according to the theory developed by O'Brien.[26–27] The particles motion is represented by the dynamic mobility, μ_d, which implies a time delay Δt between the applied field and the particle motion; μ_d is the analogue of the electrophoretic mobility in a static electric field, μ_e. The dynamic mobility takes into account the phase difference (phase lag) between the alternate electric field and the particle motion: at low frequencies Δt is zero and μ_d is equal to μ_e. The phase lag occurring at high frequencies is due to particle inertia and depends on particle size. For this reason, the dynamic mobility measurement allows to get both ζ-potential and particle size distribution values. In particular, ζ-potential was determined by fitting the particle-averaged dynamic mobility over a range of 13 different frequencies (ranging from 1 to 18 MHz) of the alternate electric field imposed. The particle-size distribution, necessary for the fitting, is also measured by a sound attenuation technique.

Data concern three kinds of ζ-potential:
(1) electrophoretic ζ-potential, that is extracted from the mobility calculated at low frequency (1.3 MHz) without correction for particle inertia;
(2) ESA ζ-potential, that is fitted with an ESA-based particle size measurement;
(3) Attenuation ζ-potential, that is fitted with an attenuation-based particle size measurement.

The latter is the more reliable value and it is given in most cases. When particle size is very small, the inertia effect cannot be estimated and the Hückel electrophoretic ζ-potential is given. The ESA ζ-potential was given when the attenuation based fitting did not converge.

To get the particle contribution to the total attenuation, the attenuation in the glycol solvent was measured and the result subtracted to the sample measurement (*background correction*).

The electric conductivity of nano-inks was measured with the dip conductivity probe (with a constant cell of 74.8) associated to the Acoustosizer after calibration with 0.01 and 0.1 M KCl solutions.

2.7. Optical Spectroscopy

The optical absorption spectra were recorded using a UV-Visible-NIR double-beam spectrophotometer (λ35, Perkin Elmer, Wellesley, USA) in the 200–1100 nm range, step 0.3 nm, using the pure solvent as a reference. Samples were diluted to an ink:glycol ratio = 1:20 and put in a quartz cuvette.

2.8. Ink-Jet Printing Tests

The technological behaviour was assessed by applying the nano-inks on two unfired substrates for ceramic tiles: a porcelain stoneware body and a bright glaze for double-fire porous tiles. The application was performed through a laboratory ink-jet printer (Apollo, Spectra, Lebanon, USA). After firing in industrial roller kilns at the proper temperature (~1100 °C for porous tiles; ~1200 °C for porcelain stoneware) the colour of ceramics was measured by diffuse reflectance spectroscopy (Miniscan MSXP4000, Hunter-Lab, Reston, USA) in the 400–700 nm range (illuminant D_{65}, observer 10°) taking a white glazed tile as a reference (CIE $x = 31.5$, $y = 33.3$). Colour is expressed in the CIELab parameters: brightness (L^* = white+, black−) and chroma (a^* = red+, green−; b^* = yellow+, blue−).

3. RESULTS AND DISCUSSION

3.1. Particle Size Distribution

The particle size of the dispersed pigments is in the 20–80 nm range, as measured by dynamic light scattering

(DLS) or 10–40 nm according to microscopic observations (Fig. 1 and Table I). These data confirm the efficiency of the polyol method in synthesizing nanoparticles regardless pigment composition.[18–19]

The particle size distribution is similar in the Black, Cyan and Yellow inks, whose particles range between 10 and 30 nm, with average values around 20 nm. On the other hand, the Magenta ink is coarser, being the gold particles in the 20–80 nm range (Fig. 1 and Table I).

The higher the pigment loading, the coarser the particle size: increasing the concentration up to 12 wt%, particle size grows from 5–8 nm to approximately 20 nm for both the Yellow and Black inks (Fig. 2(A)). This trend is confirmed by the monotonic shift of the band edge towards higher energy with decreasing pigment loading in the absorption spectra of the yellow inks (Fig. 2(B)) that may be due to agglomeration phenomena.[28]

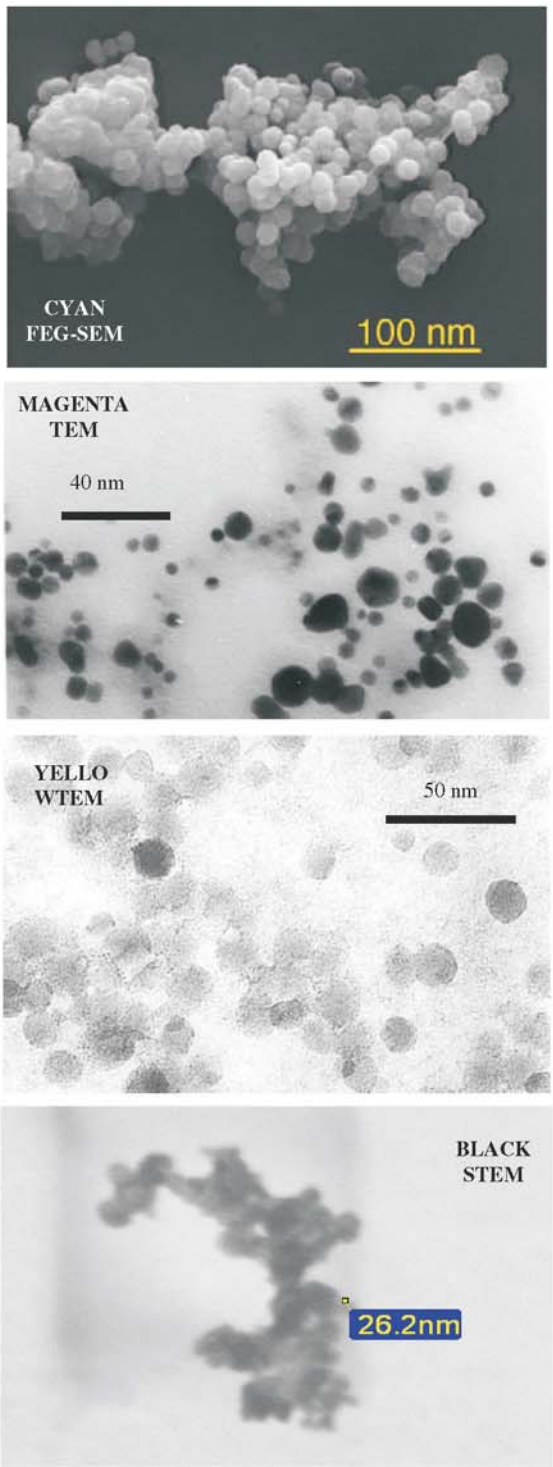

Fig. 1. TEM, STEM or SEM-FEG micrographs of the pigments dispersed in the inks.

3.2. Phase Composition

The phase composition of the four pigments dispersed in the nano-inks is as follows:

— The Black ink consists of spinel-like cobalt ferrite ($CoFe_2O_4$);

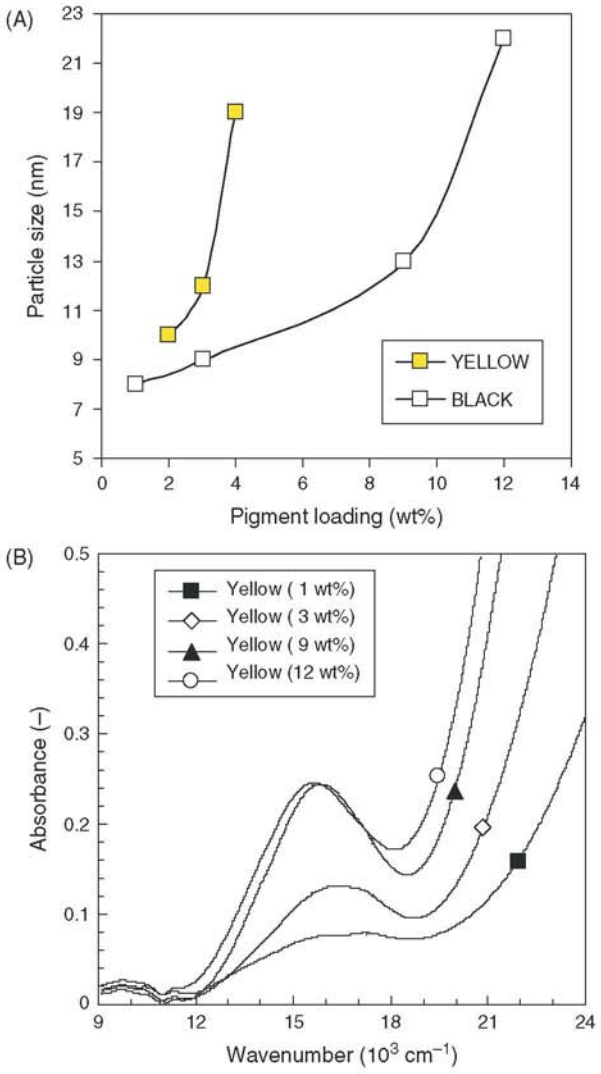

Fig. 2. Dependence of particle size on pigment loading by DLS in the Yellow and Black inks (A) and by optical spectroscopy in the Yellow ink (B).

RESEARCH ARTICLE

— The Magenta ink contains metallic gold;
— The pigment in the Cyan ink is a mixture of cobalt oxides with different oxidation states;
— The Yellow ink is peculiar, bearing anatase at room temperature, though its presence is revealed by X-ray diffraction only over 300 °C, as a consequence of the particle size growth with temperature (Fig. 3). During heating, anatase transforms in rutile, that is the desired phase to get a yellow-coloured pigment.[29] This transition occurs in between 500 and 600 °C, therefore at a considerably lower temperature than that recorded in micrometer-sized, chromium- and antimony-doped anatase.[29]

3.3. Shear Viscosity

The ink flow in the channels of the printhead must be very fast in order to make quicker both the ejection of droplets from the nozzles and the subsequent filling of the shot-chambers. Both the high flow velocity (about 20 $m \cdot s^{-1}$)[2] and the small diameters of nozzles (ranging typically from 20 to 120 μm) give shear rate of the order of magnitude of $10^5 \div 10^6$ s^{-1}. In those flow conditions, the ink viscosity must be as low as possible. In this study, the investigation of the flow behaviour was limited to shear rates of 1–100 s^{-1}. In that range, the nano-inks have shown (at 25 °C) a Newtonian behaviour with viscosities ranging from about 40 to 200 mPa·s (Fig. 4). The oscillating values measured at the lowest shear stresses applied are due to the low signals registered with the plate–plate geometry adopted.

The viscosities of nano-inks are relatively higher with respect to the typical values for ink-jet printing technology. In fact, the inks based on soluble salts have usually a viscosity between 1 and 10 mPa·s, while the viscosity

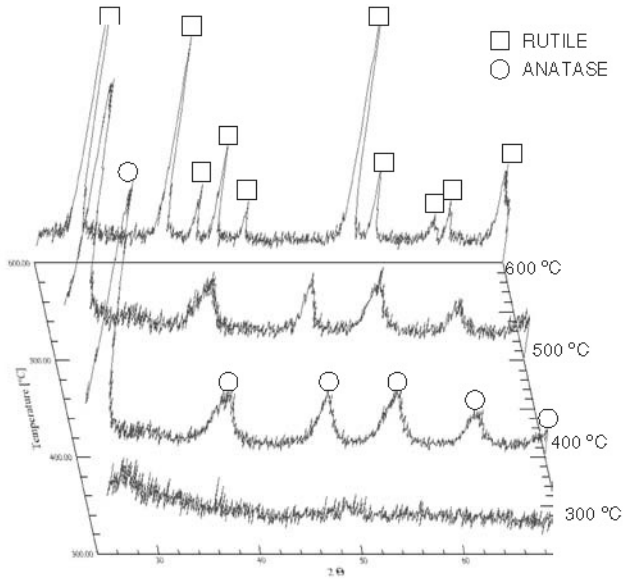

Fig. 3. HT-XRD patterns of the Yellow ink recording the anatase-to-rutile transformation in between 500 and 600 °C.

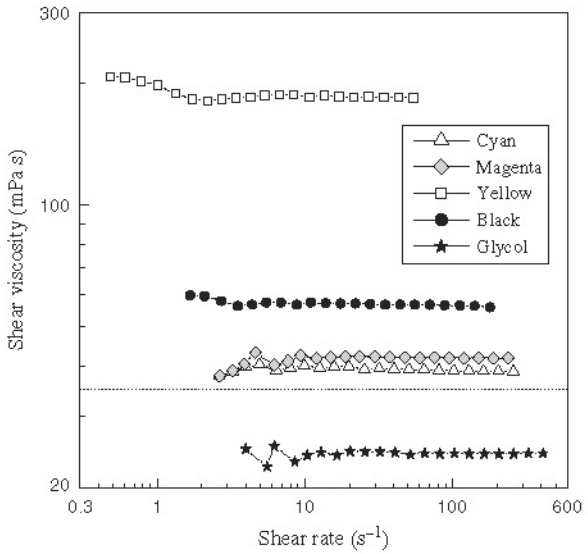

Fig. 4. Flow curves at 25 °C for nano-inks and glycol.

of the inks based on micronized pigments—although with appropriate printers it can reach also 100 mPa·s—often has to be below 35 mPa·s.[3,13] Assuming this value as the cutoff viscosity, all the nano-inks considered are out of range. In particular, the Cyan and Magenta inks have a similarly low viscosity (around 40 mPa·s) close to the limit; the Black ink has a slightly higher viscosity, about 60 mPa·s (though the Black ink is fifty times more concentrated as volume solid content than the Magenta one), while the Yellow ink has a viscosity around 190 mPa·s, hence widely out of the range for ink-jet applicability.

In order to fulfil the constraint on viscosity, a possible way is to dilute the inks to reduce the solids content, provided that saturated colors are developed anyway. However, even in this case, as the glycol used as dispersing medium has a viscosity of about 24 mPa·s (at 25 °C), the dilution is not enough to go below this limit. Another possibility is to change the operating conditions (e.g., temperature) exploiting the option to heat the inks in ink-jet printers. A third way to reduce the viscosity is to modify the physical system (e.g., adding proper additives that limit the agglomeration phenomena or replacing the glycol with another dispersing medium of lower viscosity). However, as the glycol is not a simple dispersing medium, but it also plays a key role in the synthesis of nano-inks by the polyol method, it is hardly replaceable. In this work we considered the first two ways.

The effect of solid loading on viscosity was studied with reference to the Yellow and Black inks, which were the more concentrated and viscous ones. The effect of solid content on shear viscosity of these inks is shown in Figure 5. Both the inks increase their viscosity passing from 1 to 12 wt% of solid loading, but the Yellow ink does it more quickly than the Black one. This suggests that the colloidal stability of the Yellow ink is worse than

RESEARCH ARTICLE

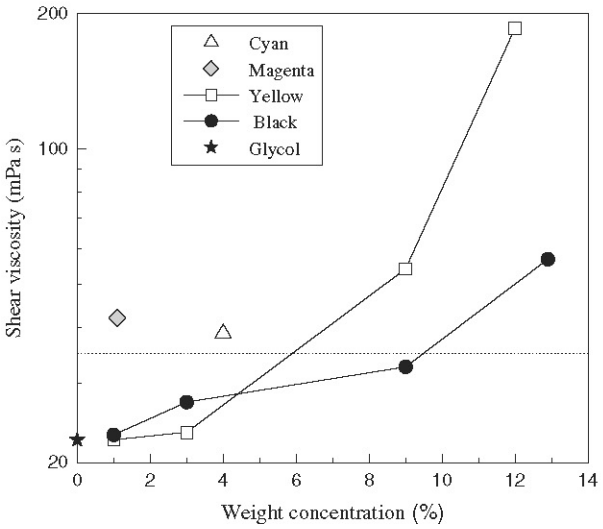

Fig. 5. Effect of solid content on viscosity of the Yellow and Black inks.

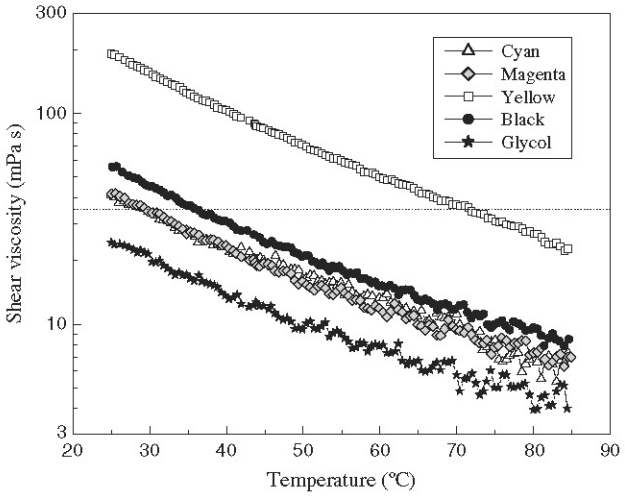

Fig. 6. Dependence of viscosity on temperature for nano-inks and glycol.

that of the Black one, i.e., the agglomeration phenomena are more favourite for titania nanoparticles with respect to cobalt ferrite ones. As shown in Figure 5, the Black ink lowers its viscosity under the cutoff value at a concentration of 9 wt%, while the Yellow ink requires a dilution down to 6 wt% which could compromise the development of a suitable saturated colour.

More effective is the reduction of viscosity by heating, that does not alter the solid content. The viscosity decrease roughly follows the same exponential decay for all the inks (Fig. 6). In first approximation, the data can be described by an Arrhenius-like exponential law which can be written in the following form:

$$\eta = \eta_{25\ ^\circ C} \exp\left[-B\left(\frac{1}{T} - \frac{1}{298.15}\right)\right] \qquad (1)$$

where $\eta_{25\ ^\circ C}$ is the ink viscosity at 25 °C, B is a parameter characteristic of each ink and T is the absolute temperature. In second approximation, as the B-parameters for the inks are quite similar, it is possible to obtain a single-parameter equation considering a mean value for B ($B_{mean} = -3460.5$ K). In this way the equation requires only the knowledge of the ink viscosity at 25 °C. As shown in Figure 6, in order to decrease the ink viscosity under the cutoff value of 35 mPa · s, it is necessary to heat the Cyan and Magenta inks to 30 °C, the Black ink to 36 °C and the Yellow ink to 72 °C.

3.4. Surface Tension

The surface tension is another physical parameter to control in order to obtain printable inks. In particular values lower than 35 mN · m^{-1} are not advisable to avoid ink wetting of the surfaces around nozzles or dripping effect by gravity from nozzles and to ensure a sufficient stability of droplets during their flight towards the substrates.[3] On the other hand, the surface tension has to be low enough to permit the droplets formation under the deformation of the piezoelectric actuator. In the literature, the suitable range for surface tension is in between 20 and 70 mN · m^{-1}.[13] The static surface tension, i.e., for droplets fully developed, changes with time in the nano-inks, decreasing until an equilibrium value is reached. This kind of behaviour is common for colloidal dispersions and it is mainly due to the nano-particles diffusion to the liquid-air interface[30] and to the contamination by the environment. Taking into account this phenomena of droplet ageing and the need to consider a parameter that is relevant for the ink-jet printing process, the value of surface tension immediately after the droplet formation out of the needle was considered, i.e., after 40 ms, corresponding to the maximum rate of image acquisition of the optical device (Table I).

The effects of both solid loading and temperature on this "initial" static surface tension were evaluated for the nano-inks. About the dependence on the content of solid particles, an increase of solid loading at low concentrations causes a decrease of surface tension due to the spontaneous diffusion of nanoparticles toward the ink-air interface that reduces the cohesion between the molecules of glycol (Fig. 7). However, a peculiar behaviour was observed for the Yellow ink: over a critical concentration, which is in the range 9–12 wt%, the surface tension returns to rise for the prevailing effect of the capillary forces between the particles at the interface.[30] The solid loading at which this behaviour is observed depends on the composition of particles. For the Black ink, further measurements showed that the increase occurs at higher concentrations. In order to make sure that the surface tension does not decrease too much at the temperatures necessary to get the optimal viscosity, its dependence on temperature was determined. The surface tension decreases for all the inks when the temperature increases, but it keeps values over 35 mN · m^{-1}

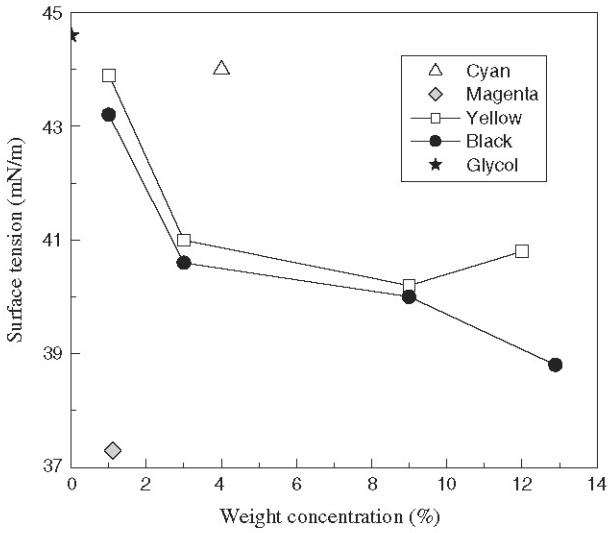

Fig. 7. Effect of solid content on surface tension of the Yellow and Black inks.

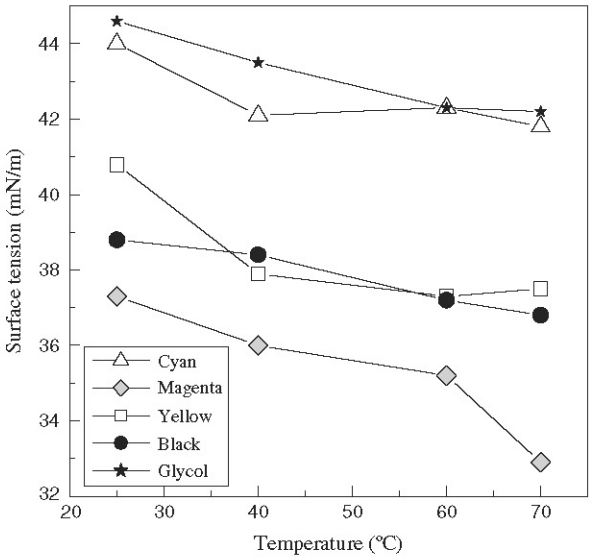

Fig. 8. Dependence of surface tension on temperature for nano-inks and glycol.

at the temperatures needed to achieve the desired viscosity (Fig. 8).

From the preceding discussion, it is clear that the fluid dynamics of drop-on-demand jets is controlled by the viscous and surface forces acting on the droplets. These two critical factors can be grouped in a dimensionless number, Z, as suggested from the studies on this field.[31] The Z number is defined as the ratio between the Reynolds number and the square root of the Weber number:

$$Z = \frac{Re}{We^{1/2}} = \frac{\sqrt{\gamma \rho a}}{\eta} \tag{2}$$

being

$$Re = \frac{\rho v a}{\eta} \tag{3}$$

$$We = \frac{\rho v^2 a}{\gamma} \tag{4}$$

where γ, η and ρ are surface tension, viscosity and density of the ink, respectively; v is a characteristic velocity of the fluid and a is a characteristic dimension, e.g., the diameter of nozzles.

On the basis of numerical simulations, it was found that the ink-jet printing is effective when the parameter Z is in between 1 and 10.[32] In substance, when Z is lower than 1, the viscosity is too high to permit the droplets ejection while, when Z is higher than 10, the high surface tension hinders the droplets formation and can cause the production of a large number of small-sized droplets rather than one of the designed size. On the basis of this simple criterion, assuming a nozzle diameter of 50 μm and neglecting the dependence of density on temperature, it is found that at 25 °C only the Cyan and Magenta inks are printable (having $1 < Z < 10$) while the Yellow and Black inks could not be printable (being $Z < 1$). Pure glycol at 25 °C has $Z = 2.1$. Increasing the temperature, the Z-parameter increases for all the systems; at the cutoff temperatures for optimal viscosity (i.e., 30 °C for Cyan and Magenta, 72 °C for Yellow and 36 °C for Black) Z is in the desired range for all the inks (Fig. 9). Obviously, increasing the diameter of nozzles, Z increases and correspondingly does the printability of inks. However, nozzles with a wider diameter give bigger droplets with a consequent loss of image resolution.

3.5. ζ-Potential

The nano-inks are characterized by positive values of ζ-potential (Table I) indicating a proton transfer between glycol and the basic surface sites of pigments. Considering

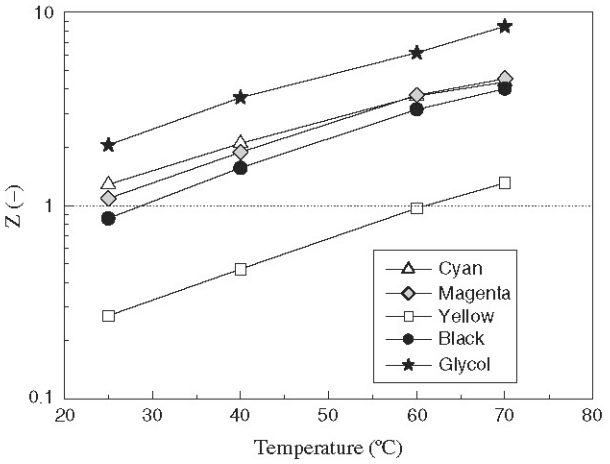

Fig. 9. Dependence of Z-parameter on temperature for nano-inks and glycol.

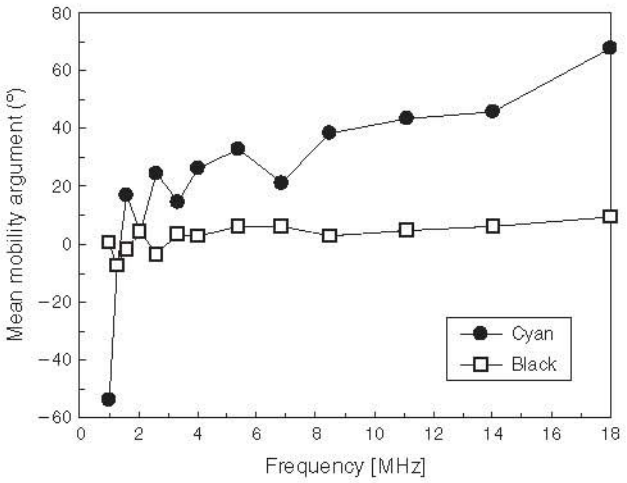

Fig. 10. Mean mobility argument of the Cyan and Black inks.

that the electrostatic repulsion potential depends on the product of the dielectric constant for the square of surface potential, it can be predicted that in the glycol medium, with a dielectric constant of about 30, the surface potential should be 1.5 times more that in water (dielectric constant about 80) to provide the same repulsion.[33] So, if 30 mV is a potential adequate in water, 45 mV is expected to be adequate in glycol to achieve an electrostatic stabilization. The ζ-potential values here measured ensure a good electrostatic stabilization in the case of the Magenta and Black inks. The good colloidal stability observed in the other cases is justified by a steric stabilization mechanism that will be discussed in details for the Cyan ink.

The ζ-potential value depends also on the occurrence of other species, that may come from the synthesis (e.g., water, surfactants); so it is reasonable comparing the values of samples differing for pigment loading but coming from the same synthesis batch. For instance, in the case of the Yellow ink, the higher loadings (i.e., Y 9% and Y 12%) were obtained starting from the Y 6% by a solvent extraction step that reduced the amount of water too. A decrease of ζ-potential is observed by increasing the pigment concentration: +60.5 mV (Y 12%), +31.4 mV (Y 9%), +20.3 mV (Y 6%); these results imply that protons adsorbed onto the pigment surface come from water, besides glycol.

The low ζ-potential value of the Cyan ink does not match the excellent colloidal stability observed. In this

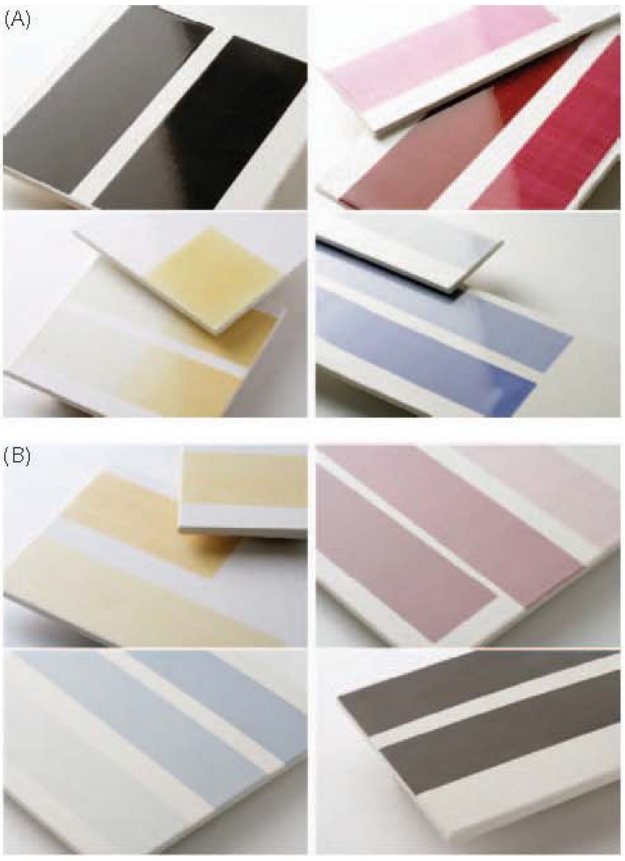

Fig. 11. Preliminary ink-jet printing tests of nano-inks on glazed tiles (A) and porcelain stoneware tiles (B).

case, a steric contribution to the stabilization may be deduced by the analysis of the dynamic mobility argument (phase angle) spectra as a function of frequency (Fig. 10). The mobility argument of the Cyan ink increases with frequency, implying the presence of organic units or polymers adsorbed on the surface, giving rise to a steric stabilization. The resulting inertia effect is a positive phase lag, increasing with frequency, that can be explained by a thick elastic layer extending out from the particle surface. This layer is reasonably formed by species that come from the precursors used in the synthesis.[21] This behaviour is not observed in the case of the Black ink, where the mobility argument shows the expected flat trend versus frequency, typical of nano-particles.

Table II. Colourimetric properties of nano-inks applied on ceramic tiles.

		Nano-ink			
Property	Unit	Cyan	Magenta	Yellow	Black
Colour (CIE-Lab)	L*	52.4 ± 0.8	37.0 ± 1.1	79.9 ± 2.1	14.2 ± 0.9
in bright glaze	a*	+10.3 ± 1.0	43.4 ± 0.2	1.8 ± 1.2	+3.1 ± 0.1
	b*	−35.1 ± 2.0	4.4 ± 1.1	47.2 ± 1.8	−6.4 ± 1.0
Colour (CIE-Lab)	L*	63.3 ± 1.1	56.1 ± 0.5	80.7 ± 0.9	35.6 ± 0.8
in porcelain stoneware	a*	−3.3 ± 0.1	17.7 ± 0.3	1.8 ± 0.7	+0.4 ± 0.1
	b*	−11.9 ± 0.7	2.5 ± 0.1	35.5 ± 2.3	+0.8 ± 0.1

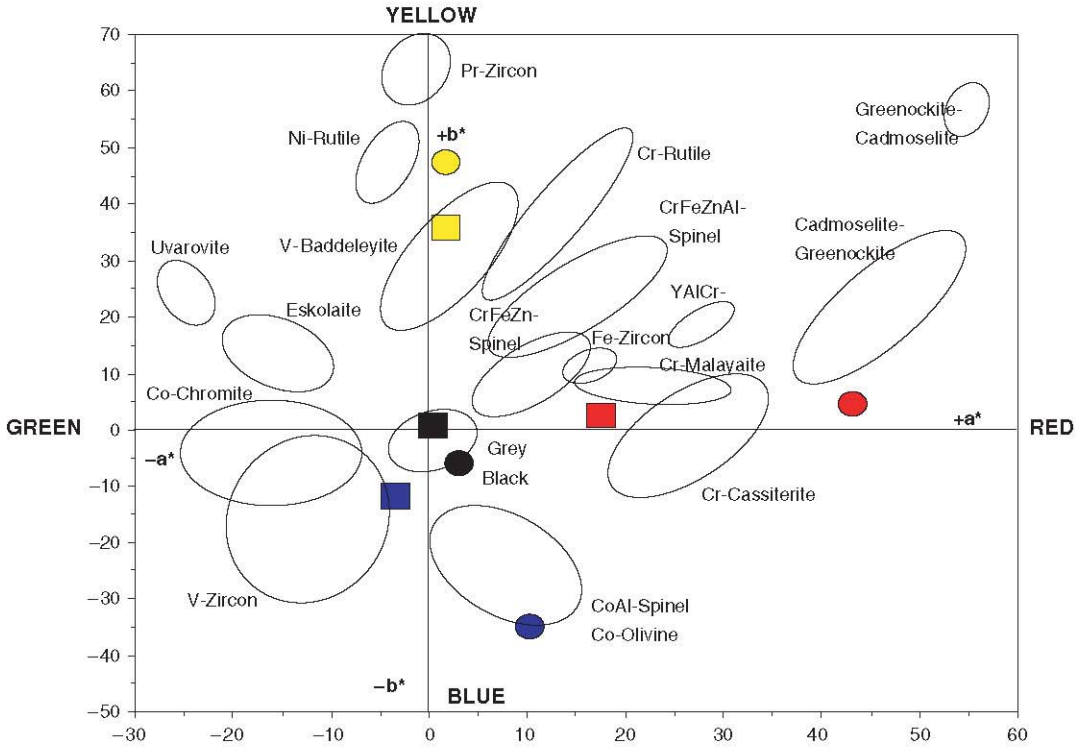

Fig. 12. Colour plot (CIELab) of industrial ceramic pigments compared to nano-inks applied on bright glaze (circles) and porcelain stoneware body (squares).

3.6. Electric Conductivity

Electrical conductivity values are in the 10–100 $\mu S \cdot cm^{-1}$ range (Table I) hence much lower than those for continuous ink-jet printing.[34–35] The Magenta ink is an exception, whose high conductivity is typical of a metal dispersion when the particle size is over 10 nm[20] as it is in our case. The particle loading affects the electrical conductivity of the Yellow ink, while the Black one exhibits almost steady values.

3.7. Ink-Jet Printing Tests

Preliminary testing was performed applying separately the four nano-inks in 7 cm wide strips on unfired ceramic substrates, i.e., a bright glaze for double-fire tiles and a body for porcelain stoneware unglazed tiles (Fig. 11). After firing in industrial roller kilns, at temperatures as high as 1100 °C (bright glaze) and 1200 °C (porcelain stoneware), the decorated tiles exhibit vivid and saturated colours reasonably corresponding to the quadrichromy requirements (Table II).

The colouring performance of nano-inks is close or in some cases even better than that of the ceramic pigments currently used in tilemaking.[7–8] In particular, the Cyan ink imparts a deep blue to the bright glaze, analogous to that of cobalt aluminate spinel, or a cyan shade to matt surfaces such as porcelain stoneware. The Magenta ink produces a brilliant and pure red in bright glaze (not far from the performance of cadmium sulfo-selenide) and a less vivid magenta hue (close to colours achievable with chromium-doped malayate or cassiterite) in porcelain stoneware bodies. The Yellow ink bestows similar shades on both bright and matt substrates, with a colour closer to that of vanadium-bearing zirconia than to praseodymium-doped zircon. Very dark surfaces are obtained with the Black ink, resulting in a pure black on porcelain stoneware and a bluish cast on bright glaze (Fig. 12).

4. CONCLUSIONS

Highly stable ceramic inks were prepared by the polyol method, succeeding to get pigments with actually nanometric size (i.e., between 20 and 80 nm) based on metallic gold or oxides. These pigments develop vivid colours approaching the yellow, cyan, magenta and black required for the quadrichromy printing process.

A wide-ranging characterization—including particle size distribution, phase composition, shear viscosity, surface tension, and ζ-potential—proved these inks do fulfil the requirements for the drop-on-demand ink-jet printing. Some non-optimal behaviours can be satisfactorily corrected by increasing the ink temperature before droplets ejection.

The physico-chemical properties of nano-inks depend on the concentration and chemical nature of pigments as well as on the occurrence of synthesis by-products (e.g., water).

Preliminary testing demonstrates that these nano-sized ceramic inks are fully suitable for the four-colours ink-jet printing. Further work will attempt to optimise the ink-jet application, trying to understand which phenomena occur and mostly influence the kinetics of ink penetration into the ceramic substrates.

References and Notes

1. M. Paganelli, Glazing and Decoration of Ceramic Tiles, Italian Ceramic Society, SALA, Modena **(2000)**, p. 197.
2. A. Atkinson, J. Doorbar, A. Hudd, D. L. Segal, and P. J. White, *J. Sol-Gel Tech.* 8, 1093 **(1997)**.
3. P. Calvert, *Chem. Mater.* 13, 3299 **(2001)**.
4. H. P. Lee, *J. Imaging Sci. Technol.* 42, 49 **(1998)**.
5. V. Lázaro, A. García, I. Fuentes, and J. Clausell, *Proc. 7th World Congr. Ceramic Tile Quality QUALICER*, Castellón, Spain **(2004)**, p. 189.
6. S. Obata, H. Yokoyama, T. Oishi, M. Usui, O. Sakurada, and M. Hashiba, *J. Mater. Sci.* 39, 2581 **(2004)**.
7. R. A. Eppler, *Am. Ceram. Soc. Bull.* 66, 1600 **(1987)**.
8. Italian Ceramic Society, Glazing and Decoration of Ceramic Tiles, SALA, Modena **(2000)**.
9. A. L. Costa, G. Cruciani, M. Dondi, and F. Matteucci, *Ind. Ceram.* 23, 1 **(2003)**.
10. H. R. Kang, *J. Imag. Sci.* 35, 179 **(1991)**.
11. B. Y. Tay and M. J. Edisiringhe, *J. Mater. Res.* 16, 373 **(2001)**.
12. B. Y. Tay and M. J. Edisiringhe, *Proc. R. Soc. Lond. A* 458, 2039 **(2002)**.
13. X. Zhao, J. R. G. Evans, M. J. Edirisinghe, and J. H. Song, *Ceram. Int.* 29, 887 **(2003)**.
14. D. Gardini, F. Matteucci, M. Blosi, M. Dondi, A. L. Costa, C. Galassi, M. Raimondo, G. Baldi, and E. Cinotti, *Proc. 8th World Congr. Ceramic Tile Quality QUALICER*, Castellón, Spain **(2006)**, p. 397.
15. M. Dondi, F. Matteucci, D. Gardini, M. Blosi, A. L. Costa, C. Galassi, G. Baldi, A. Barzanti, and E. Cinotti, *Adv. Sci. Technol.* 51, 174 **(2006)**.
16. C. Feldmann, J. Merikhi, and H.-O. Jungk, *J. Mater. Chem.* 10, 1311 **(2000)**.
17. C. Feldmann and H.-O. Jungk, *Angew. Chem. Int. Ed.* 40, 359 **(2001)**.
18. L. Poul, S. Ammar, N. Jouini, F. Fiévet, and F. Villain, *J. Sol-Gel Sci. Tech.* 26, 261 **(2003)**.
19. M. Fernandez-Garcia, A. Martinez-Arias, J. C. Hanson, and J. A. Rodriguez, *Chem. Rev.* 104, 4063 **(2004)**.
20. C. N. R. Rao, A. Müller, and A. K. Cheetham, The Chemistry of Nanomaterials, Synthesis, Properties and Applications, Wiley-VCH, Weinheim-Berlin **(2005)**.
21. G. Baldi, M. Bitossi, and A. Barzanti, Patent WO 03/076521 A1 **(2003)**.
22. A. C. Larson and R. B. Von Dreele, *Los Alamos Nat. Lab. Rep. LAUR* **(2000)**, p. 86.
23. H. Toby, *J. Appl. Crystallogr.* 34, 210 **(2001)**.
24. R. J. Hunter, *Colloids and Surf. A* 141, 37 **(1998)**.
25. R. W. O'Brien, D. W. Cannon, and W. N. Rowlands, *J. Colloid Interface Sci.* 173, 406 **(1995)**.
26. R. W. O'Brien, *J. Fluid. Mech.* 190, 71 **(1988)**.
27. R. W. O'Brien, *J. Fluid. Mech.* 212, 81 **(1990)**.
28. C. N. R. Rao, G. U. Kulkarni, P. J. Thomas, and P. P. Edwards, *Chem. Eur. J.* 8, 28 **(2002)**.
29. F. Matteucci, G. Cruciani, M. Dondi, and M. Raimondo, *Ceram. Int.* 32, 385 **(2006)**.
30. L. Dong and D. Johnson, *Langmuir* 19, 10205 **(2003)**.
31. J. E. Fromm, *IBM J. Res. Develop.* 28, 322 **(1984)**.
32. N. Reis and B. Derby, *Mater. Res. Soc. Symp. Proc. Solid Freeform and Additive Fabrication* 625, 117 **(2000)**.
33. M. Fowkes, *Adv. Ceram.* 21, 411 **(2003)**.
34. W. D. Teng and M. J. Edirisinghe, *Key Eng. Mater.* 132, 337 **(1997)**.
35. H. M. Nur, J. H. Song, J. R. G. Evans, and M. J. Edirisinghe, *J. Mater. Sci. - Mater. in Electr.* 13, 213 **(2002)**.

Received: 20 December 2006. Accepted: 21 June 2007.